ANL/NE-16/13

Rate Theory Modeling and Simulation of Silicide Fuel at LWR Conditions

Nuclear Engineering Division

About Argonne National Laboratory
Argonne is a U.S. Department of Energy laboratory managed by UChicago Argonne, LLC under contract DE-AC02-06CH11357. The Laboratory's main facility is outside Chicago, at 9700 South Cass Avenue, Argonne, Illinois 60439. For information about Argonne and its pioneering science and technology programs, see www.anl.gov.

DOCUMENT AVAILABILITY

Online Access: U.S. Department of Energy (DOE) reports produced after 1991 and a growing number of pre-1991 documents are available free via DOE's SciTech Connect (http://www.osti.gov/scitech/)

Reports not in digital format may be purchased by the public from the National Technical Information Service (NTIS):
U.S. Department of Commerce
National Technical Information Service
5301 Shawnee Rd
Alexandria, VA 22312
www.ntis.gov
Phone: (800) 553-NTIS (6847) or (703) 605-6000
Fax: (703) 605-6900
Email: **orders@ntis.gov**

Reports not in digital format are available to DOE and DOE contractors from the Office of Scientific and Technical Information (OSTI):
U.S. Department of Energy
Office of Scientific and Technical Information
P.O. Box 62
Oak Ridge, TN 37831-0062
www.osti.gov
Phone: (865) 576-8401
Fax: (865) 576-5728
Email: **reports@osti.gov**

Disclaimer
This report was prepared as an account of work sponsored by an agency of the United States Government. Neither the United States Government nor any agency thereof, nor UChicago Argonne, LLC, nor any of their employees or officers, makes any warranty, express or implied, or assumes any legal liability or responsibility for the accuracy, completeness, or usefulness of any information, apparatus, product, or process disclosed, or represents that its use would not infringe privately owned rights. Reference herein to any specific commercial product, process, or service by trade name, trademark, manufacturer, or otherwise, does not necessarily constitute or imply its endorsement, recommendation, or favoring by the United States Government or any agency thereof. The views and opinions of document authors expressed herein do not necessarily state or reflect those of the United States Government or any agency thereof, Argonne National Laboratory, or UChicago Argonne, LLC.

ANL/NE-16/13

Rate Theory Modeling and Simulation of Silicide Fuel at LWR Conditions

prepared by
Yinbin Miao, Bei Ye, Zhi-Gang Mei, Gerard Hofman, and Abdellatif Yacout
Nuclear Engineering Division, Argonne National Laboratory

Kyle Gamble
Fuel Modeling and Simulation, Idaho National Laboratory

prepared for
U.S. Department of Energy
Nuclear Energy Advanced Modeling & Simulation Program

September 1, 2016

ABSTRACT

As a promising candidate for the accident tolerant fuel (ATF) used in light water reactors (LWRs), the fuel performance of uranium silicide (U_3Si_2) at LWR conditions need to be well-understood. In this report, rate theory model was developed based on existing experimental data and density functional theory (DFT) calculations so as to predict the fission gas behavior in U_3Si_2 at LWR conditions. The fission gas behavior of U_3Si_2 can be divided into three temperature regimes. During steady-state operation, the majority of the fission gas stays in intragranular bubbles, whereas the dominance of intergranular bubbles and fission gas release only occurs beyond 1000 K. The steady-state rate theory model was also used as reference to establish a gaseous swelling correlation of U_3Si_2 for the BISON code. Meanwhile, the overpressurized bubble model was also developed so that the fission gas behavior at LOCA can be simulated. LOCA simulation showed that intragranular bubbles are still dominant after a 70 second LOCA, resulting in a controllable gaseous swelling. The fission gas behavior of U_3Si_2 at LWR conditions is benign according to the rate theory prediction at both steady-state and LOCA conditions, which provides important references to the qualification of U_3Si_2 as a LWR fuel material with excellent fuel performance and enhanced accident tolerance.

CONTENTS

ABSTRACT iv
1. Rate Theory Model for Fission Gas Bubble Evolution 1
2. Steady-State Model Parameterization 4
3. Power Transient Model Parameterization 6
4. Steady-State and Power Transient LWR Conditions 7
4.1 Steady-State Operation Parameters 7
4.2 Models for Peripheral Parameters 7
4.3 LOCA Conditions in LWRs 9
5. Steady-State Fission Gas Behavior without Cladding 11
5.1 Rate Theory Modeling Results 11
5.2 Development of Rate Theory Based Correlation for the BISON code 14
6. Steady-State Fission Gas Behavior with Cladding 16
7. Fission Gas Behavior at LOCA 19
7.1 Zero Hydrostatic Stress Case 19
7.2 Hydrostatic Stress from BISON 21
8. Conclusions 23
9. Acknowledgements 24
10. References 25

FIGURES

Figure 4.1 Mesh used in the BISON-based LOCA simulation 8
Figure 4.2 Power history of each element in the BISON-based LOCA simulation 9
Figure 4.3 Temperature history of each element in the BISON-based LOCA simulation 9
Figure 4.4 Hydrostatic stress history of each element in the BISON-based LOCA simulation ... 10
Figure 5.1 Three temperature regimes of fission gas behavior in U_3Si_2 11
Figure 5.2 Bubble size and number density at different temperatures and temperature gradients 12
Figure 5.3 Effect of element number within LWR temperature range (T stands for the average fuel temperature) 13
Figure 5.4 Three temperature regimes of fission gas behavior in U_3Si_2 in 10-element simulation 13
Figure 5.5 Bubble size and number density at different temperatures and temperature gradients in 10-element simulation 14
Figure 6.1 Comparison between the rate theory simulation and the BISON correlation 16
Figure 6.2 Bimodal size distribution of intragranular fission gas bubbles 17
Figure 6.3 Evolution of the hoop stress and creep displacement of the cladding 17
Figure 7.1 Swelling behavior in all the eleven elements with zero hydrostatic stress 19
Figure 7.2 Detailed gas swelling profile after the LOCA 19
Figure 7.3 Intragranular bubble size distribution before the LOCA at 40,000 MWd/tU: (left) bubble size distribution from 0.2 nm to 100 nm in radius; (right) bubble size distribution near the large size peak. 20
Figure 7.4 Intragranular bubble size distribution after the LOCA at 40,000 MWd/tU: (left) bubble size distribution from 0.2 nm to 100 nm in radius; (right) bubble size distribution near the large size peak. 20
Figure 7.5 Intragranular bubble size distribution throughout the fuel life cycle (left) bubble size distribution from 0.2 nm to 100 nm in radius; (right) bubble size distribution near the large size peak. 21
Figure 7.6 Comparison between zero stress and BISON stress conditions 21
Figure 7.7 Intragranular bubble size distribution throughout the fuel life cycle with BISON-based stress (left) bubble size distribution from 0.2 nm to 100 nm in radius; (right) bubble size distribution near the large size peak. 22

TABLES

Table 1.1 values of parameters used in the calculations 2
Table 2.1 Values of key parameters in the rate theory model used by the GRASS-SST code..... 4
Table 4.1 LWR conditions adopted in this study[6] 7
Table 6.1 Sensitivity analysis on key parameters at LWR conditions (Ref: ΔV/V=5.2265%) 18

1. Rate Theory Model for Fission Gas Bubble Evolution

Argonne National Laboratory (ANL) has developed two fuel performance codes based on the rate theory, GRASS-SST and DART, for the simulation of fission gaseous swelling behavior in nuclear fuels. While the GRASS-SST (Gas Release and Swelling Subroutine – Steady State and Transients) code focuses on the evolution of fission gas atom itself and therefore suits the mission of dealing with monolithic form of fuels, the DART (Dispersion Analysis Research Tool) code was designed for handling dispersion form of fuels by involving models capturing the interactions between fuel particles and aluminum matrix. In this report, as we concentrate on using monolithic U_3Si_2 fuels in LWRs, GRASS-SST was employed to perform all the rate theory simulations.

GRASS-SST models the effects of fission-product generation, atomic migration, bubble nucleation and re-solution, bubble migration and coalescence, interlinked porosity, and fission-gas interaction with structural defects [1]. GRASS-SST calculates the fission-gas-bubble-size distribution for bubbles in the lattice, on grain boundaries, on dislocations, and along the grain edges by solving a set of coupled nonlinear differential equations as expressed below:

$$\frac{dC_i^\alpha}{dt} = -a_i^\alpha C_i^\alpha C_i^\alpha - b_i^\alpha C_i^\alpha + e_i^\alpha \qquad (i = \mathbf{1}, \ldots, \mathrm{N};\ \alpha = 1, 2, 3, 4), \tag{1-1}$$

where i is the number of atoms in a bubble; C_i^α is the number density of α-type bubbles in the i th-size class; α = 1, 2, 3, 4 represents the location of the bubbles at the lattice, dislocation, grain-face, and grain-edge, respectively; and the coefficients a_i^α, b_i^α, and e_i^α represent the rates at which α-type bubbles are lost or added to the i th-size class through assorted processes (bubble coalescence, migration process, re-solution/generation, etc.)[1]. Each one of the coefficients a_i^α, b_i^α and e_i^α is dependent on multiple materials properties, such as gas atom diffusivities and gas bubble nucleation and resolution rates. The key materials properties that impact fission gas behavior most, and their values used in this study are listed in Table 1.1. Detailed description of those materials properties and determination of their values will be presented in Sections II and III.

Those key parameters that determine the gaseous swelling behavior of nuclear fuels can be further categorized in to two types: lattice related material properties and grain boundary related material properties. The former mainly accounts for the evolution of intragranular fission bubbles, while the latter controls the kinetics of intergranular fission bubbles and gas release. Aside from those material properties, external environment parameters, such as temperature, temperature gradient, fission rate, and hydrostatic pressure, also considerably influence the procedures of fission bubble evolution.

The fission-gas-induced swelling is due to the formation of gas bubbles within fuel during irradiation. In GRASS-SST, the fission-gas-induced swelling $(\frac{\Delta V_{fuel}}{V_{fuel}^0})_g$ is calculated as the summation of gas bubble volumes at all locations and in all size classes, which is

$$(\frac{\Delta V_{fuel}}{V_{fuel}^0})_g = \sum_{i=1}^{N}\sum_{\alpha=1}^{4} C_i^\alpha v_i^\alpha \tag{1-2}$$

where v_i^α is the volume of α-type bubbles in the i th-size class. As the rate theory model only distinguishes the number of fission gas atoms contained by a bubble, the volume of that bubble is

determined by a specific equation of state (EOS). For instance, modified hard sphere EOS is adopted by GRASS-SST to calculate the size of a bubble contain a specific number of gas atoms:

$$\frac{4}{3RT}\pi r^3(p+2\gamma/r)=Z^{hs}(y)-d\,v_0\,f(T)-\Delta Z\,, \qquad (1\text{-}3)$$

where, p is the hydrostatic pressure, γ is the surface energy of the fuel material, r is the radius of the bubble assuming a spherical shape, T is the thermodynamics temperature. The right hand size (RHS) of Equation 1-3 accounts for the amount of substance of gas atoms in the bubbles and the effects of hard sphere atomic potential, which was described in Ref. [2]

Table 1.1 values of parameters used in the calculations

Category	Parameter	Symbol	Unit
Lattice material properties	Pre-exponential coefficient in gas atom diffusivity	$D_0 (D_g = D_0 \exp(-\frac{Q}{kT}))$	cm^2/s
	Activation energy for gas atom diffusion	Q	cal
	Radiation-enhanced gas atom diffusivity factor	D_g^{RED} $(D_g^{tot} = D_g + D_g^{RED}\dot{f})$	cm^5
	Bubble nucleation factor on grain boundaries	f_n	N/A
	Resolution rate in lattice	$b_0 (b = b_0 \dot{f})$	cm^3
	Fuel surface energy	γ	erg/cm^2
Grain boundary material properties	Multiplication factor to obtain effective irradiation-induced resolution of gas atoms from grain face	$gbr(1)$ $(b_{grainboundry} = gbr(1) \cdot b_0 \cdot \dot{f})$	N/A
	Enhancement factor for gas atom irradiation-enhanced diffusion on grain boundaries	ξ	N/A

Besides the retention of fission gases in fuel, GRASS-SST also accounts for fission gas release from fuel. During fission gas release process, gas atoms diffuse from the grains to grain boundaries and then to the grain edge, where the gas is released through a network of interconnected tunnels of fission-gas and fabrication porosity. The observed formation of grain-surface channels is also modeled, in addition to providing a direct path through which gas residing on the grain surface can reach the grain edges, contributing to intergranular separation and/or cause long-range pore interlinkage. In the fuel temperature regime in this work, there are no bubble movements involved, which become active at very

high temperatures (> 1500°C). For the U_3Si_2 fuel system analyzed in this study, the stresses on cladding are mainly caused by fission-gas-induced swelling not fission gases released from fuel.

The other component of fuel swelling is solid fission product swelling in addition to fission gas swelling. For solid fission product swelling, no experimental measurements are available. Therefore, estimates are made based on the atomic volume differences between solid fission products and fission-consumed uranium atoms. Solid-fission-product-induced swelling is modeled as linearly proportional to fission density and largely independent on fuel type and temperature. The formulation of $(\frac{\Delta V_{fuel}}{V_{fuel}^0})_{sp}$ can be written as:

$$(\frac{\Delta V_{fuel}}{V_{fuel}^0})_{sp} = \alpha F_d \,, \qquad (1\text{-}4)$$

where $(\frac{\Delta V_{fuel}}{V_{fuel}^0})_{sp}$ is in %, α is a constant, and F_d is fission density in 10^{21} fissions/cm^3. In this study, α is equal to 1.38, which is suggested by Hofman and Ryu[3] for U_3Si_2 dispersion fuel for test reactors.

2. Steady-State Model Parameterization

In comparison to the operation in research reactors, fuels in LWRs experience elevated temperatures. Thus, thermally-activated diffusion of Xe plays an important role in the fission gas behavior at LWR conditions, whereas radiation-enhanced diffusion (RED) of Xe is dominant at research reactor conditions. The diffusivity of a single Xe atom in U_3Si_2 has been assess by means of DFT using Vienna Ab-initio Simulation Package (VASP) with projector augment-wave (PAW) method and Perdew-Burke-Ernzerhof (PBE) potentials for the exchange-correlation potentials. In a monoclinic structure crystal such as U_3Si_2, migration of a Xe atom through a-b plane and c-axis differentiates due to the asymmetric atomic structure. A series of possible migration routes were considered, the migration enthalpies of which were calculated by DFT. Assuming a single Xe atom incorporated in U_3Si_2 has entropy of $5k_B$, where k_B is the Boltzmann constant, the diffusivity of Xe through a specific migration route ca be calculated and compared with those through other routes. It was found that the migration of a Xe atom from one U vacancy to another U vacancy along c-axis overwhelmingly dominates the diffusion of Xe in U_3Si_2, whereas the diffusion of Xe through the a-b plane is suppressed. As a result, the Xe diffusion in U_3Si_2 is actually a one-dimensional diffusion, namely, $\mathbf{D} = \mathrm{diag}\{0,0,D_3\}$. TO take this anisotropy into account, an effective three-dimensional diffusivity, $D_{eff} = D_3/3$, was used in the GRASS-SST rate theory model, where spherical grain shape and three-dimensional Xe diffusion are assumed. In fact, the adoption of the effective three-dimensional diffusivity yields the same steady-state Xe concentration in this rate theory model with a uniform Xe source term. In this study, $D_0 = 7.73\times10^{-7}$ m^2/s and Q = 1.68 eV.

As shown in Equation 1-3, the size of fission gas bubbles is determined by the surface energy of the fuel material to a considerable extent. Hence, a credible estimate of the surface energy of U_3Si_2 is crucial for the accurate prediction of the gaseous swelling strain. Unfortunately, due to the lack of related references, little knowledge on the surface energy of U_3Si_2 can be learned from existing experimental database. Thus, DFT calculation was utilized to calculate the surface energy of a series of surfaces with various Miller indices. The DFT calculation was performed using the same parameters as described early in this report. The surface energy was found to vary from 1.16 J/m^2 to 1.48 J/m^2, depending on the crystallographic orientation of the surface. For instance, the {100} surface has a surface energy of 1.48 J/m^2, while the {001} surface has a surface energy of 1.43 J/m^2. For the sake of simplicity, an average surface energy of 1.32 J/m^2 was used in this study for all the fission gas behavior simulation at LWR conditions.

Table 2.1 Values of key parameters in the rate theory model used by the GRASS-SST code

Parameters	D_o	Q	D_g^{RED}	f_n	b_0	γ	$gbr(1)$	χ
Unit	m^2/s	eV	m^5	n/a	m^3	J/m^2	n/a	n/a
Value	7.73×10^{-7}	1.68	1.0×10^{16}	0.01	1.0×10^{-25}	1.32	1.00	2000

Although abundant in-pile irradiation data are available for U_3Si_2, the majority of those results were obtained at the research reactor conditions[4]. That is, those existing data usually involve a lower irradiation temperature (<300°C) and higher fission density (related to the higher enrichment) in comparison to irradiation experiments at LWR conditions. At those research reactor conditions, the gas bubbles are invisible in scanning electron microscopy (SEM) images until the fission density exceeds a threshold value. This threshold or so-called "knee" phenomenon might be connected to the amorphization and recrystallization procedures. At LWR conditions, however, U_3Si_2 is expected to maintain its monoclinic crystal structure throughout its entire approximately 5% burnup lifetime. Consequently, only those experimental data measured prior to the threshold were taken into consideration to deduce the rate theory parameters. The research reactor data were used to fit those rate theory parameters that can hardly assessed by DFT calculations. In those research reactor data prior to the threshold, intragranular bubbles dominate the gaseous swelling, whereas the contribution from

intergranular bubbles can be neglected. Additionally, as all those research data involve the dispersion fuel form, where the U_3Si_2 particles were embedded in Al matrix, a 1233 psi hydrostatic stress was assumed, which equals the effective yield stress of Al considering the radiation creep.

Based on the computational and experimental approaches described above, the values of those key parameters of the GRASS-SST rate theory model during steady-state operation were determined and are listed in Table 2.1. The sensitivity analysis of those parameters has been reported in Ref. [5].

3. Power Transient Model Parameterization

Unlike the steady-state simulation, additional dynamic procedures need to be taken into consideration in the GRASS-SST rate theory model in order to simulate power transients. Growth of fission gas bubbles is driven by the bubbles absorbing vacancies from matrix medium. During steady state, growth of bubbles is slower than the diffusion of vacancies. Thus, the bubble size during steady state is equal to its equilibrium size. As power transients occur, however, diffusion of vacancies may not be adequate for immediate bubble growth. Namely, overpressurized bubbles are likely to exist in the transient state simulations. The growth of those overpressurized bubbles is governed by diffusion creep of the matrix. The growth rate is described in the GRASS-SST model:

$$\frac{dr}{dt} = \frac{D_v C_v}{r}\left[1 - \exp\left(-\frac{p^{ex}\Omega}{k_B T}\right)\right], \tag{3-1}$$

where, r is bubble radius, t is time, D_v is vacancy diffusivity, C_v is equilibrium concentration of vacancies, p^{ex} is the extra pressure of the bubble compared to the equilibrium state, k_B is Boltzmann constant, and T is thermodynamic temperature.

On the other hand, during the LOCA, the temperature actually drops first due to the loss of power and then rises to a higher level due to the thermal insulation. During the temperature drop, gas bubbles are under-pressurized and subject to shrink. Gas bubble shrinkage has two possible mechanisms: interstitial absorption and vacancy emission. During the LOCA, as fission power is zero, interstitial absorption is the dominant mechanism. Thus, a bubble shrinkage model was established using an equation similar to Equation 3-1. The only difference is that the shrinkage is controlled by interstitial self-diffusion rather than the vacancy self-diffusion. The diffusivities of both interstitials and vacancies of U_3Si_2 were calculated using the DFT with the same setup as in Xe diffusivity calculation. The diffusion mechanism of uranium vacancy and interstitial with highest corresponding diffusivities were selected to be the estimates of the parameters controlling the growth and shrinkage during power transients: $D_{o,v}$ = 7.53×10^{-6} m^2/s, Q_v = 2.13 eV, $D_{o,i}$ = 1.05×10^{-5} m^2/s, and Q_i = 1.68 eV.

Additionally, in the rate theory model embedded in the GRASS-SST code, overpressurized bubbles have different diffusion mechanism from equilibrium bubbles. The diffusivity of equilibrium bubbles was derived from the diffusivity of a single Xe atom as described in the GRASS-SST code manual, while the diffusion of overpressurized bubbles is enhanced by surface diffusion. At general conditions, the diffusivity of a fission gas bubble originates from both diffusion mechanisms. The fraction of either mechanism is determined by the extra pressure, p^{ex}, of that bubble and temperature rising rate. For this part of the rate theory model, due to the lack of experimental and computational data for the surface diffusion in U_3Si_2, related parameters were adopted from the existing well-developed UO_2 model.

4. Steady-State and Power Transient LWR Conditions

4.1 Steady-State Operation Parameters

LWRs operate at higher temperatures and achieve lower fuel burnup compared to research reactors. In order to examine the fuel performance of U_3Si_2 in LWRs, the conditions adopted by the GRASS-SST code must be adjusted accordingly. For consistency and simplicity, the LWR conditions used by the BISON group at Idaho National Laboratory (INL) were adopted in this study. Some key LWR conditions are listed in Table 4.1.

Table 4.1 LWR conditions adopted in this study[6]

Parameter	Unit	Value
Linear average power	W/cm	200
Fast neutron flux	$n/m^2 \cdot s$	9.50×10^{17}
Coolant pressure	MPa	15.5
Coolant temperature	K	530
Fill gas initial pressure	MPa	2.0
Initial fuel density	%	95
Power	MW/tU	35.28
Maximum Burnup	MWd/tU	45000

Cylinder fuel pellets without reserved central void were clad by Zircaloy-4. The Zr alloy cladding was selected rather than advanced cladding solution such as SiC or FeCrAl to provide direct comparison with the conventional UO_2-Zr solution. In fact, the ongoing in-pile irradiation of U_3Si_2 at the Advanced Test Reactor (ATR) also involves the ZIRLO as the cladding material for U_3Si_2. The pellet has a 8.2 mm diameter. Between the pellets and the cladding was an 80 μm gap, which is filled with 2.0 MPa helium gas. Detailed temperature profile and other operation data were adopted from Ref. [6]. The steady-state analysis was performed with a constant power for 3.2 years to a final burnup of 45,000 MWD/tU.

4.2 Models for Peripheral Parameters

Aside from the RT model described above, other simplified models were also involved in the fine swelling simulations at LWR conditions to capture those peripheral parameters. The details of those models are discussed as follows.

First of all, the He fill gas changes its pressure due to the temperature fluctuation and fuel swelling throughout the fuel life-cycle. This change in pressure controls the external hydrostatic pressure of the fuel, especially prior to the gap closure. As the pressure and temperature of the He gas are not extreme, ideal gas equation of state was used to govern this procedure:

$$pV = nRT \ . \tag{4-1}$$

The helium gas was assumed to maintain 650K constant temperature, while the gas volume is determined by the combined effect of cladding creep-down and fuel swelling.

The fuel densification model was adopted from the previous BISON simulation. In this ESCORE model, the densification strain, ε_D, has the following expression[6]:

$$\varepsilon_D = \Delta\rho_0 \left(e^{\int_0^{Bu} \frac{dt}{Bu_D} \frac{\ln(100)}{C_D(t)}} - 1 \right), \tag{4-2}$$

where $\Delta\rho_0$ is the maximum densification, Bu is the burnup, Bu_D is the burnup point where the maximum densification occurs, C_D is a temperature dependent parameter:

$$C_D = \begin{cases} 7.2 - 0.0086(T - 298) & T \le 750K \\ 1 & T > 750K \end{cases}, \tag{4-3}$$

T is thermodynamic temperature.

The thermal expansion coefficient of the U_3Si_2 fuel was selected as 1.50×10^{-6} K^{-1}[6][7]; the solid fission product swelling rate is 1.38% per 10^{21} f/cm^3, as mentioned before.

The Zorcaloy-4 cladding was assumed to maintain a constant average temperature of 590K. Thus, the Young's modulus is 86.2 GPa, whereas the yield strength is 145 MPa. After yielding, the cladding was assumed to experience perfect plastic deformation without any working hardening. The radiation creep rate, $\dot{\varepsilon}$ (percent per hour), was governed by Watkin's empirical model for Zircaloy [8] (only secondary stage was considered):

$$\dot{\varepsilon} = 3.98\times10^{-15}\phi^{0.85}\sinh\left(1.67\times10^{-2}\sigma\right)\exp\left(-14000/RT\right), \tag{4-4}$$

where ϕ is the fast neutron (>1 MeV) flux (n/m2·s), σ is the stress (MPa), R is the gas constant (1.987 cal/k·mol), and T is the thermodynamic temperature (K).

The fuel temperature has a difference of 190K between the centerline and the surface and a parabolic shape as discussed before. The surface temperature was assumed to be a linear function of the gap width.

In order to couple the GRASS-SST code with those peripheral models, the code was modified to enable the restart function. The latest version of the GRASS-SST code stores all the variables after each timestep. The code can restart based on those stored data and alteration of those data between timesteps is possible. It is worth mentioning that this code update not only enables the coupling of those peripheral models, but also get the GRASS-SST code prepared for prospective coupling with BISON through MOOSE platform.

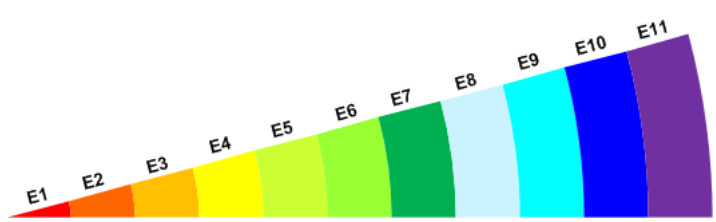

Figure 4.1 Mesh used in the BISON-based LOCA simulation

4.3 LOCA Conditions in LWRs

The LOCA simulation in this study utilizes parameters calculated by the BISON code[9]. In the BISON-based LOCA simulation, the base simulation was run for approximately 40,000 MWD/tU average burnup prior to the introduction of the LOCA. The U_3Si_2 pellet was divided into 11 elements in the radial direction, as shown in Figure 4.1. The power history of each element can be found in Figure 4.2. Here, the linear power of each element was normalized to the entire pellet cross-section for direct comparison across different elements. It is prominent that outer elements have higher power density as they are closer to the moderator and therefore have higher thermal neutron flux. As the LOCA occurs, the reactor is immediately shutdown so that the power decreases to zero.

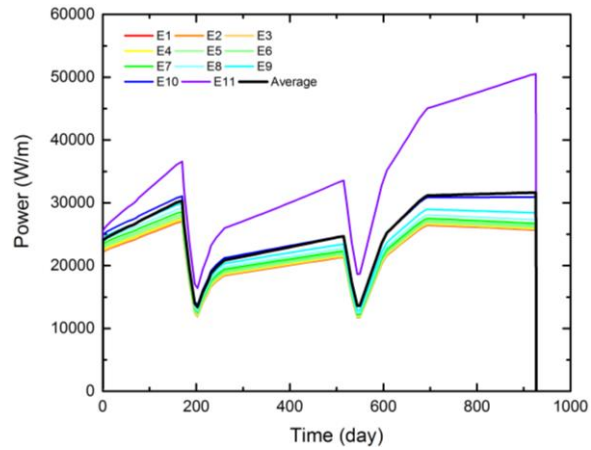

Figure 4.2 Power history of each element in the BISON-based LOCA simulation

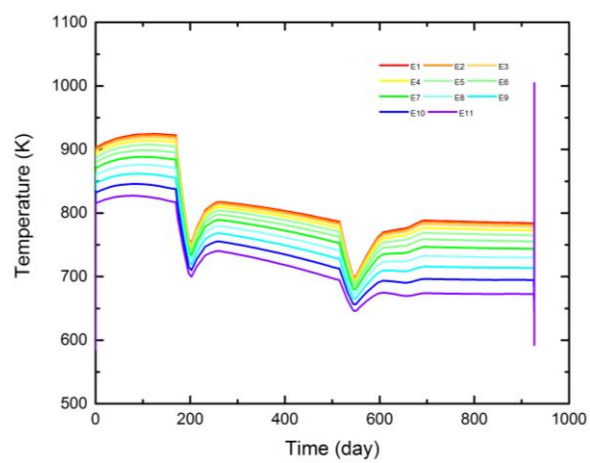

Figure 4.3 Temperature history of each element in the BISON-based LOCA simulation

Meanwhile, the temperature profile within the pellet was also calculated by the BISON code, as shown in Figure 4.3. In the beginning of the LOCA, due to the cessation of fission reactions, the temperature drops. As the absence of coolant continues, the accumulation of decay heat leads to the temperature increase up to 1,000K after merely 70 seconds (see Figure 4.3). Additionally, the hydrostatic stress within the fuel may also affect the size of fission gas bubbles by altering the gas pressure within those bubbles. The BISON simulation also includes the calculation of the hydrostatic stress profile, which is

influenced by the helium filling gas, cladding, as well as the strain field induced by temperature and power gradient within the fuel (see Figure 4.4). In the BISON code, the gas swelling model of U_3Si_2 is a simple parabola correlation derived from low temperature test reactor data, which differs from the rate theory model's prediction that is based on both experimental and computational references. As hydrostatic stress is highly related to the gaseous swelling, comparison was made with zero hydrostatic stress and the BISON-based hydrostatic stress in the study.

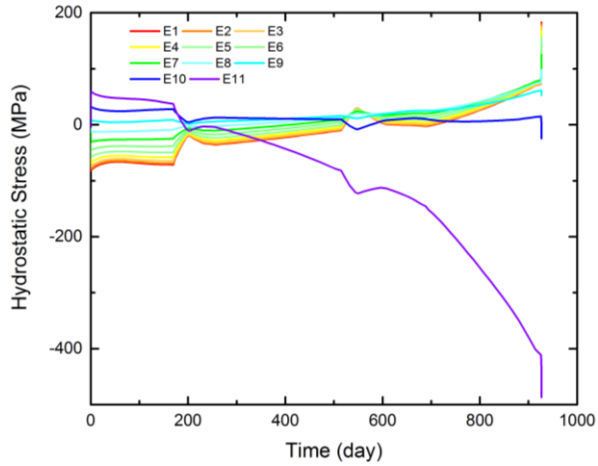

Figure 4.4 Hydrostatic stress history of each element in the BISON-based LOCA simulation

5. Steady-State Fission Gas Behavior without Cladding

5.1 Rate Theory Modeling Results

Prior to the introduction of any peripheral models, the temperature and temperature gradient effects on the fission gas behavior were first investigated. For simplicity, a single-element setup was utilized for the entire fuel pellet in the beginning. Additionally, the helium fill gas was assumed to maintain its 2 MPa initial pressure regardless to the temperature variation of the fuel pellet. A 10K interval was used to examine the fission gas behavior depending on the temperature ranging from 390K up to 1190K. Four representative temperature gradient values (G = 0, 20, 40, and 60 K/mm) were selected to study the temperature gradient effects. Thus, the gaseous swelling and fission gas release situation assessed by the GRASS-SST rate theory model at 45,000 MWD/tU is illustrated in Figures 5.1 and 5.2. The gaseous swelling strains that are contributed by the intragranular (lattice) and intergranular (grain surface and edge) bubbles were computed, and are shown separately. From 390K (research reactor temperature) through 700K (LWR temperature) up to 1190K (accident scenario), three temperature regimes can be identified according to their different fission gas behaviors. When the temperature is below approximately 750K, the gaseous swelling is comparable to that in a low-temperature research reactor before the occurrence of the "knee" point (Regime I). In Regime I, small intragranular bubbles accounts for the majority of the swelling. When the temperature exceeds 750K but is not very high (Regime II), the gaseous swelling slowly increases with the fuel temperature. Size distribution shows that this increase originates from the formation of large intragranular bubbles. The appearance of those larger intragranular bubbles also results in the bimodal size distribution of intragranular bubbles. As the fuel temperature is even higher (Regime III), the bubbles on grain boundaries start to considerably contribute to the gaseous swelling, leading to severe swelling and eventually gas release. Additionally, temperature gradient was found to influence the threshold temperature of Regime III. In the absence of temperature gradient, Regime III does not appear at up to 1190K. As temperature gradient increases to 20 K/mm, the Regime III occurs as temperature is beyond approximately 1000K. As temperature gradient continues to increase, the threshold temperature also drops slightly but stays near 1000K.

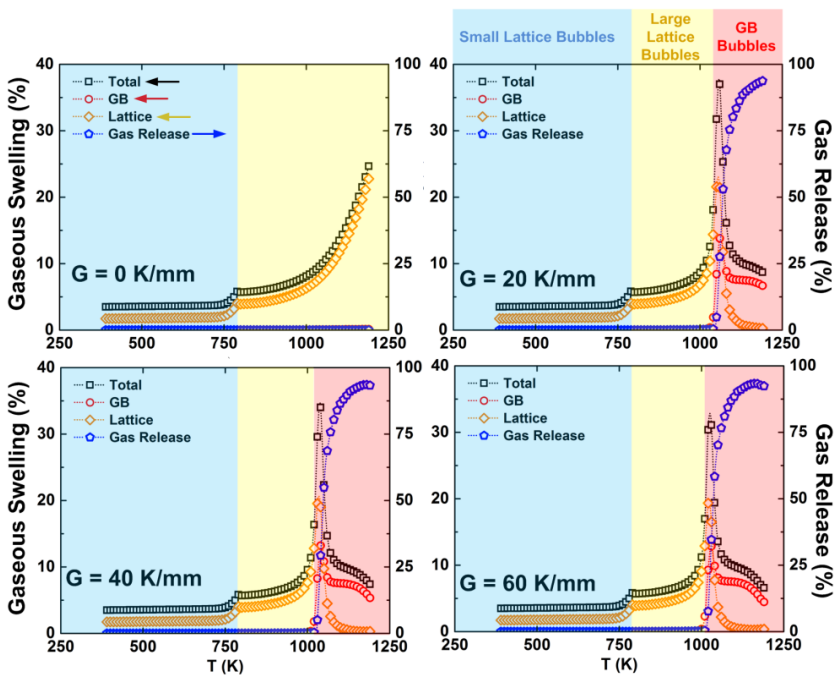

Figure 5.1 Three temperature regimes of fission gas behavior in U_3Si_2

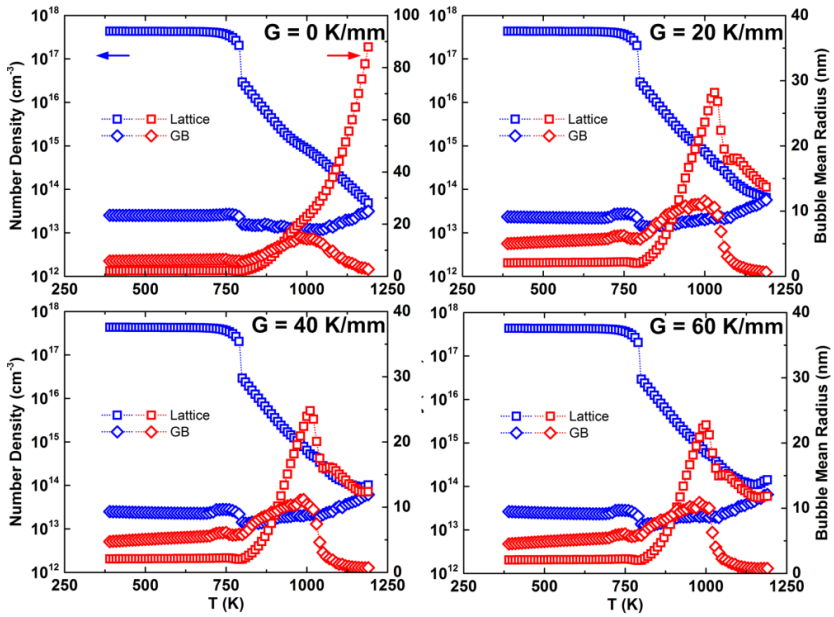

Figure 5.2 Bubble size and number density at different temperatures and temperature gradients

As mentioned previously, the parameterization of the intergranular bubbles is not dedicatedly optimized due to the lack of experimental data. Hence, the quantitative information of Regime III might not be perfectly reliable. Nevertheless, the qualitative features of the three divided regimes are credible.

Since the gaseous swelling behavior is sometimes sensitive to fuel temperature at LWR temperature and above, more elements are expected to be necessary so as to capture the bubble evolution precisely. Thus, different element numbers were tested for different temperature conditions, as shown in Figure 5.3. If the temperature profile stays in one regime, 1 element is enough to replicate the swelling behavior. However, as the temperature profile crosses two regimes, 10 elements are essential to provide convergent results. Hence, 10 elements were used for the fine swelling simulation considering all those peripheral models.

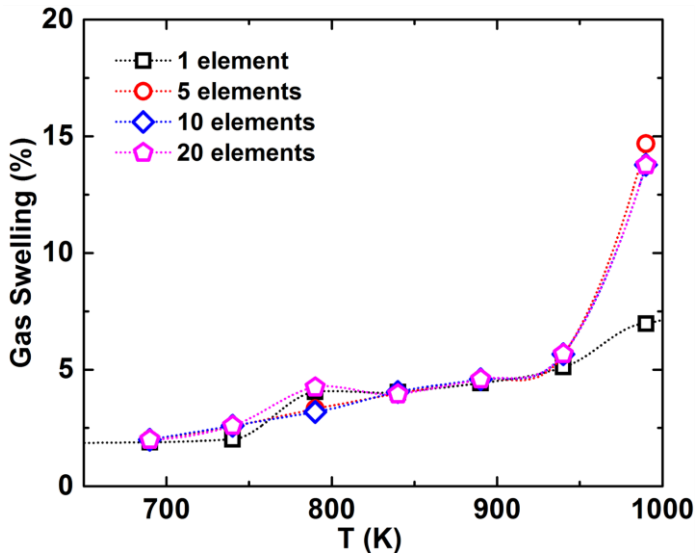

Figure 5.3 Effect of element number within LWR temperature range (T stands for the average fuel temperature)

Using the 10-element setup, the temperature dependence of the fission gas behavior was reexamined. The results are shown in Figures 5.4 and 5.5. As in the multi-element simulation, each element has its own temperature and temperature gradient. As a result, different elements may be in the different temperature regimes. As shown in Figure 5.4, the divisions between regimes are not as apparent as that in single-element simulation. More importantly, as in real fuel pellets, the high temperature part (centerline) usually has low temperature gradient, whereas the high temperature gradient part (surface) has low temperature. Considering the fact that severe gas swelling needs both sufficient temperature and temperature gradient (see Figures 5.1 and 5.2), the actual gas swelling should be lower than the estimation in single-element simulations. As the 10-element is capable of capturing this temperature-temperature gradient feature discussed above, the corresponding simulation does give a lower gas swelling strain in Regime III.

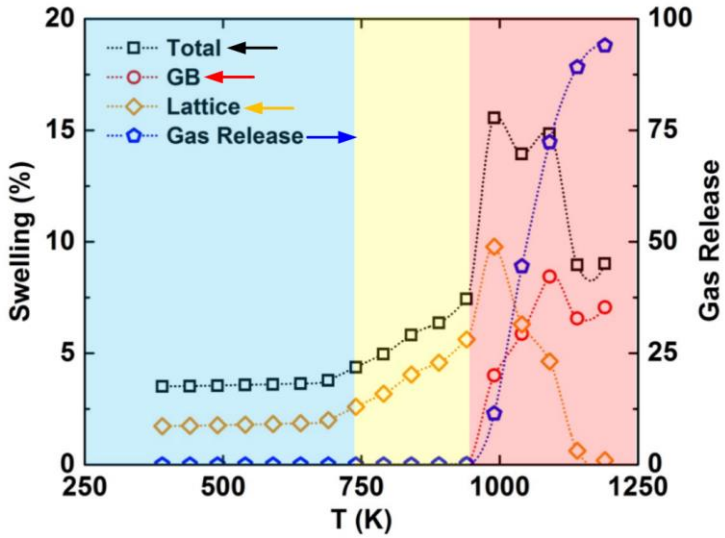

Figure 5.4 Three temperature regimes of fission gas behavior in U_3Si_2 in 10-element simulation

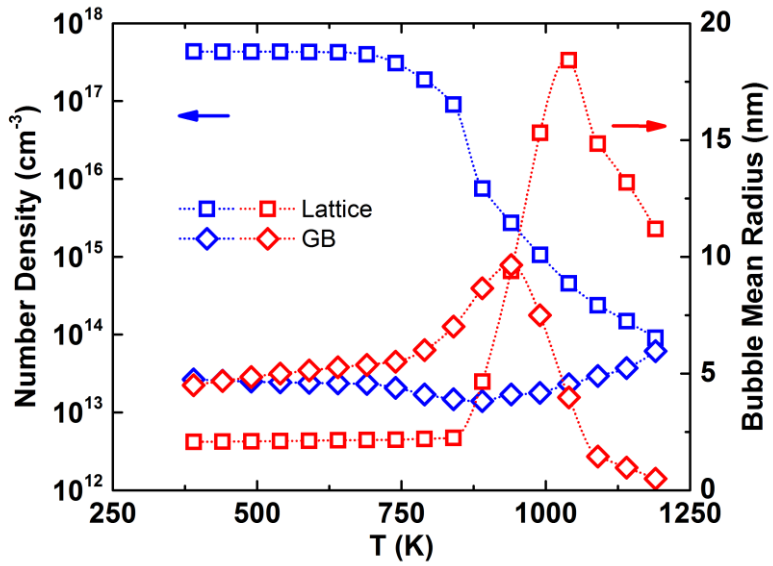

Figure 5.5 Bubble size and number density at different temperatures and temperature gradients in 10-element simulation

5.2 Development of Rate Theory Based Correlation for the BISON code

In order to improve the gas swelling model used by the BISON code, rate theory prediction of the fission gas behavior in U_3Si_2 fuel at LWR conditions has to be embedded into the BISON database. As described in the rate theory model, gaseous swelling is not only dependent to a series of different variables such as temperature, temperature gradient, burnup, fission rate, and hydrostatic stress, but also related to the existing fission gas status which is determined by the history of the fuel. Thus, the ideal way to utilize the rate theory model in BISON simulation is to couple those two codes together. However, coupling of those two codes requires both labor and time. Instead, it makes sense to first develop a gaseous swelling correlation based on the rate theory results and reasonable assumptions.

In this study, it is assumed that the gaseous swelling in U_3Si_2 is only dependent on three variables: temperature (T), temperature gradient (G), and fission density (f). Using this assumption, the temperature/temperature gradient in an element is not supposed to vary significantly. To be conservative, the highest temperature and temperature gradient during the entire fuel history can be used as the values of T and G. A typical LWR fission rate was used to generate the swelling data for fitting, so the application of this correlation should not be off the typical LWR conditions. Thus, seven temperature points (400K, 500K, 600K, 700K, 800K, 900K, and 1,000K), seven temperature gradient points (0, 12.2, 24.4, 36.6, 48.8, 61.0, and 73.2 K/mm), and up to 1.29×10^{21} fission/cm^3 fission density (~5% burnup), were used to calculate the gaseous swelling data by the GRASS-SST code. The following empirical function was used to fit the data:

$$\left(\frac{\Delta V}{V}\right)_{gaseous} = a_1 f^2 + a_2 f + a_3\left[\exp\left(a_4 f\right) - 1\right], \qquad (5\text{-}1)$$

where a_i are functions of G and T and were fitted to the rate theory results. The fitted correlation is capable of replicating the rate theory results with constant temperature and temperature gradient. This correlation has been embedded to the BISON database. Now it is still on the private version of the BISON team. Once the correlation is further validated, it will be in the public BISON database that is available to every user.

6. Steady-State Fission Gas Behavior with Cladding

By involving all those peripheral models introduced before, the steady-state fission gas behavior of U_3Si_2 at LWR conditions with cladding effect was predicted. The swelling results were compared with the correlation used in the previous BISON simulation, which was based on the low temperature research reactor experiments as shown in Figure 6.1. It is obvious that the rate theory model yields a gaseous swelling prediction that is higher than the BISON correlation at low and intermediate burnup. This is due to the fact that at LWR conditions, the temperature range almost fit Regime II in Figure 5.1. Hence, unlike the low temperature situation, the intragranular bubbles can be as large as tens of nm. The size distribution of the gas bubbles predicted by the fine swelling simulation is shown in Figure 6.2. The dominant intragranular fission gas bubbles have a bimodal size distribution as predicted by the rate theory model. The small-sized group is identical to what was observed at those low temperature research reactor conditions, while the large-sized group (tens of nm) forms due to the increasing diffusivity at elevated temperature. On the other hand, at high burnup, the BISON correlation gives gaseous swelling strains higher than the rate theory model does. This is due to the fact that the BISON correlation was developed by fitting the research reactor data which have the "knee" phenomenon. As a result, the high burnup part of the BISON correlation overestimates gaseous swelling as amorphization and recrystallization are not issues at LWR conditions. Additionally, in LWRs, the fuel temperature is not high enough to activate the prominent evolution of bubbles on grain boundaries and the consequent gas release. Here, the GRASS-SST code gives a more credible prediction of the fission gas swelling behavior compared to the simple BISON correlation, showing the advantage of the rate theory model in assessing the radiation swelling phenomenon in U_3Si_2 fuel.

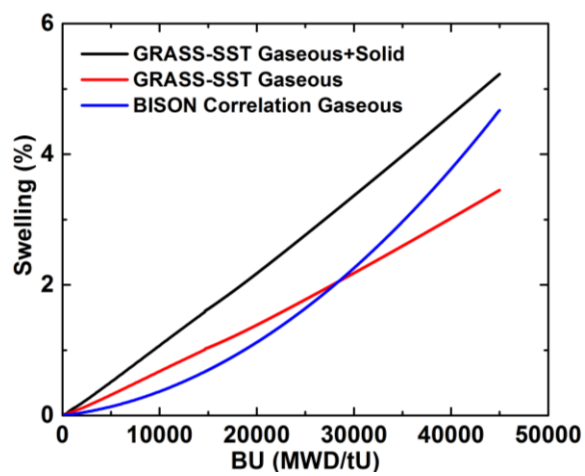

Figure 6.1 Comparison between the rate theory simulation and the BISON correlation

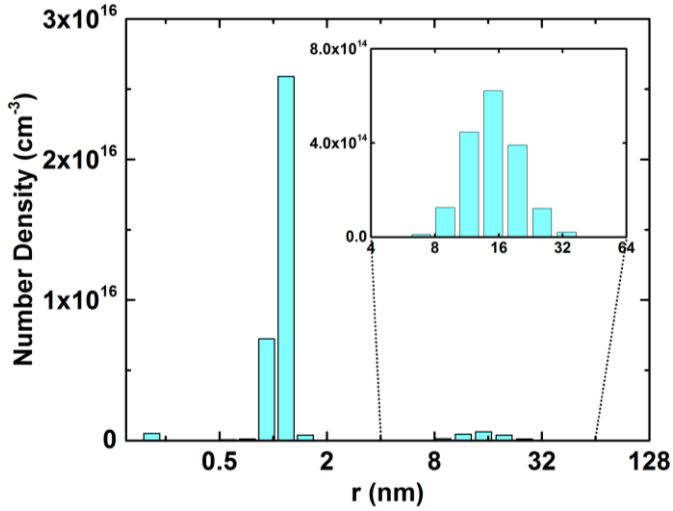

Figure 6.2 Bimodal size distribution of intragranular fission gas bubbles

Due to the swelling of the fuel and the creep-down of the cladding, gap closure occurs at approximately 14,000 MWd/tU. Soon after the gap closure, the hoop stress of the Zircaloy-4 cladding flips (see Figure 6.3), resulting in the corresponding flip of the creep direction (see Figure 6.3). As the hoop stress increases, the hydrostatic pressure of the fuel also increases (>25 MPa, or 3675 psi). However, this high pressure seems not to significantly affect the swelling behavior shown in Figure 6.1. This is because those intragranular bubbles of radii around tens of nm are still too small to be compress. Instead, the bubble size is controlled by the surface energy of the fuel.

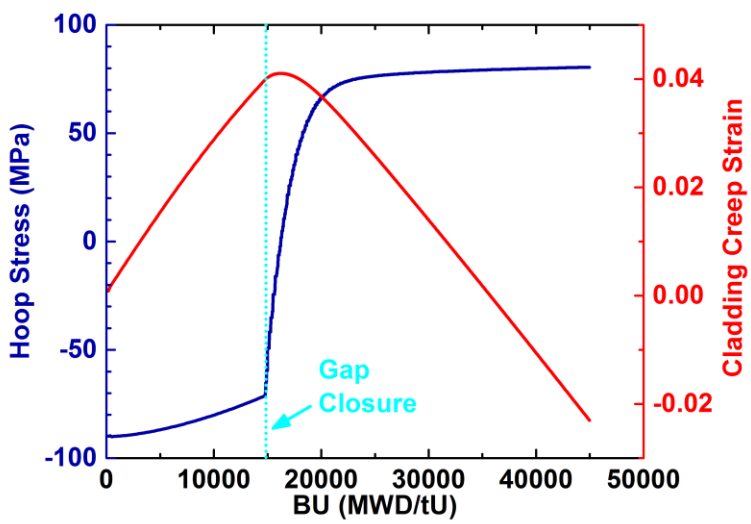

Figure 6.3 Evolution of the hoop stress and creep displacement of the cladding

The sensitivity analysis on the key parameters is shown in Table 6.1. As bubble evolution is still limited within the grains rather than on the grain boundaries, the swelling behavior at LWR conditions is still sensitive to Xe diffusivity within grains, f_n, b_0 and γ. Meanwhile, the influence of those grain boundary related parameters, gbr(1) and ξ in particular, is still marginal. At LWR temperature, thermally-activated diffusivity of Xe exceeds the radiation-enhanced diffusivity, being the dominant driving force

of bubble evolution. As a result, the swelling results become more sensitive to D_0 and Q compared to D_g^{RED}. It is worth mentioning that the constraint from the Zircaloy-4 cladding limited the swelling behavior in some cases involving prominent increase in swelling rate. For example, decrease in surface energy is supposed to lead to a large increase in swelling. However, pressure from the cladding relieves the severe inflation due to the absence of surface constraint.

Table 6.1 Sensitivity analysis on key parameters at LWR conditions (Ref: ΔV/V=5.2265%)

Parameter	Unit	Value	ΔV/V (%)
D_0	cm^2/s	7.73×10^{-2}	5.4519
		7.73×10^{-4}	5.1421
Q	cal	7.75×10^{-4}	5.1460
		1.94×10^{-4}	7.4361
D_g^{RED}	cm^5	1.0×10^{-25}	5.2723
		1.0×10^{-27}	5.1569
f_n	n/a	0.1	4.9514
		0.001	5.4851
b_0	cm^3	1.0×10^{-18}	6.1096
		1.0×10^{-20}	4.7743
γ	erg/cm^2	5000	4.0436
		200	8.9119
gbr(1)	n/a	10	5.2387
		0.1	5.2462
ξ	n/a	20000	5.2272
		200	5.2280

7. Fission Gas Behavior at LOCA

7.1 Zero Hydrostatic Stress Case

As the swelling of the fuel is interrelated with the hydrostatic stress, a zero hydrostatic stress case was first investigated to reveal the fission gas behavior without influences from the cladding. The gas swelling behavior of U_3Si_2 is illustrated in Figure 7.1. The solid fission product swelling was calculated using the empirical value of 1.38% per 10^{21} fission/cm^3. It is obvious that all the elements except for E11 have similar swelling. The extraordinary swelling of E11 originates from extra power. Before LOCA occurs, the total swelling (gaseous and solid) is approximately 5.5% after 40,000 MWd/tU burnup. Figure 7.2 shows a detailed average gas swelling profile after the LOCA. As the temperature drops in the early stage of the LOCA, even the centerline temperature has a minimum around 600K. In that case, although the fission gas bubbles are all underpressurized, the low self-diffusivity of interstitials suppresses bubble shrinkage. As the temperature rises up to 1000K, the bubbles become overpressurized, and the gas swelling increases due to the activated vacancy self-diffusion.

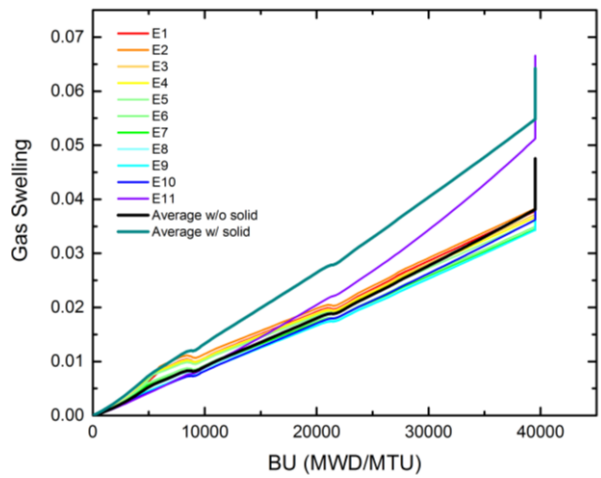

Figure 7.1 Swelling behavior in all the eleven elements with zero hydrostatic stress

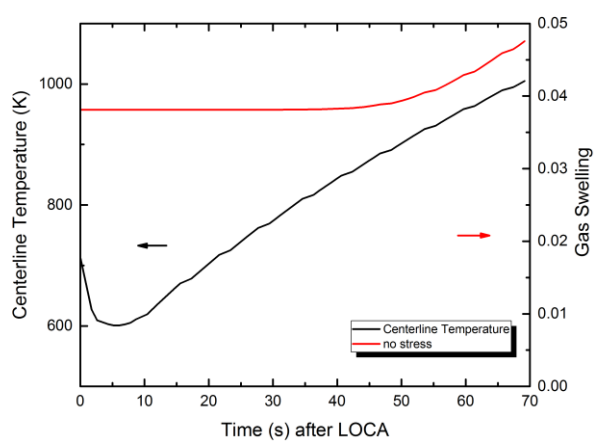

Figure 7.2 Detailed gas swelling profile after the LOCA

As discussed in the previous report, the gas swelling in U_3Si_2 at LWR conditions is dominated by intragranular bubbles. The bubble size distribution is bimodal, with two peaks near 1 nm and 20 nm, respectively. The bubble size distribution before the LOCA at 40,000 MWd/tU is consistent with the simulation results included in the previous report [1], as shown in Figure 7.3.

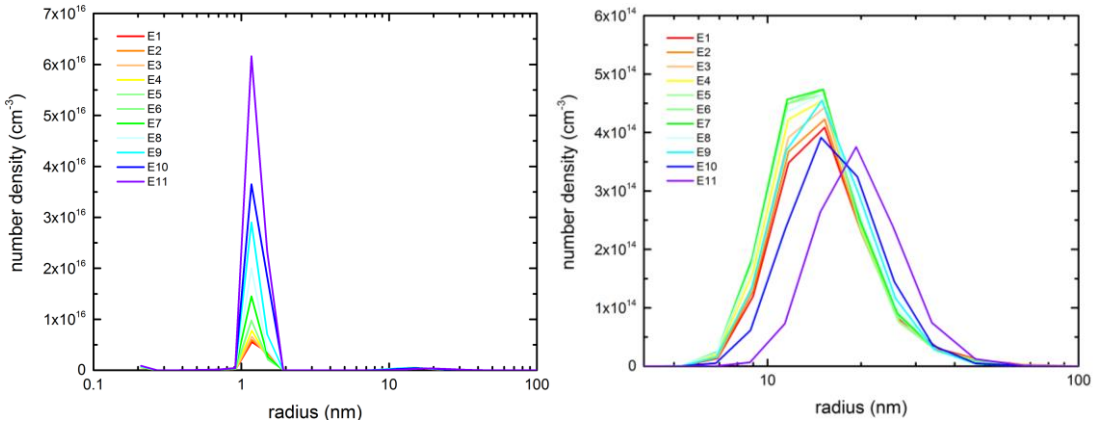

Figure 7.3 Intragranular bubble size distribution before the LOCA at 40,000 MWd/tU: (left) bubble size distribution from 0.2 nm to 100 nm in radius; (right) bubble size distribution near the large size peak.

After the LOCA, the size distribution of gas bubbles is shown in Figure 7.4. The number density of the small intragranular bubbles decreases, while the size of small intragranular bubble increases. This change is due to both the accelerated coalescence of small overpressurized bubbles and expansion of overpressurized bubbles. Meanwhile, the number density of large intragranular bubbles barely changes, whereas the size of large intragranular bubbles slightly increases. This can be explained mainly by the expansion of overpressurized bubbles due to elevated temperatures induced by the LOCA.

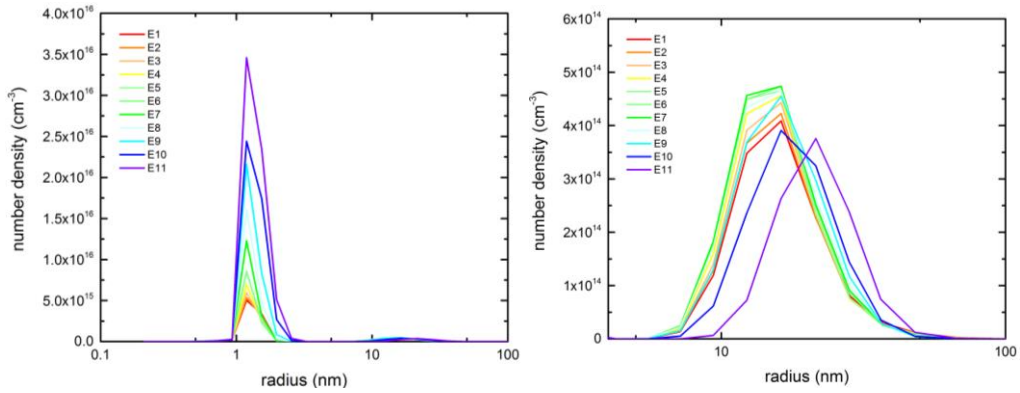

Figure 7.4 Intragranular bubble size distribution after the LOCA at 40,000 MWd/tU: (left) bubble size distribution from 0.2 nm to 100 nm in radius; (right) bubble size distribution near the large size peak.

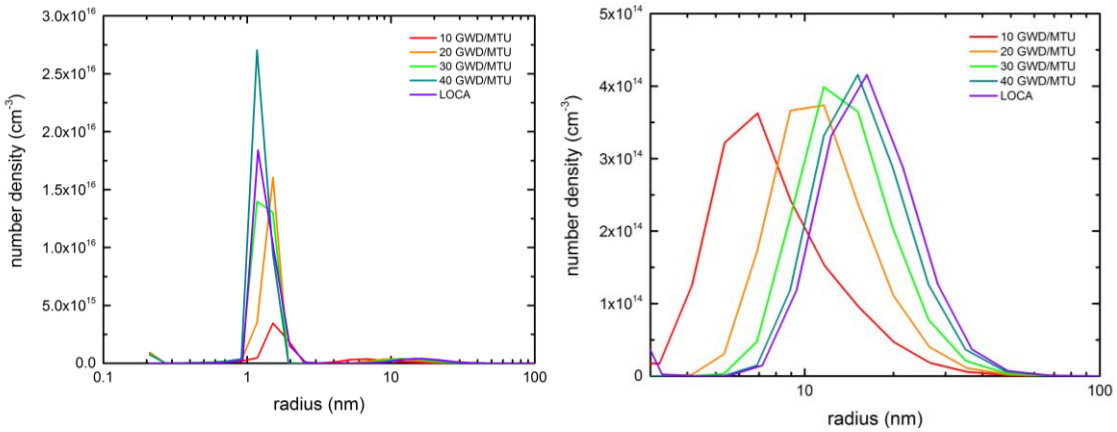

Figure 7.5 Intragranular bubble size distribution throughout the fuel life cycle (left) bubble size distribution from 0.2 nm to 100 nm in radius; (right) bubble size distribution near the large size peak.

Figure 7.5 shows the bubble size distribution averaged over all the eleven elements at several representative time points. It is obvious that the number density of the small intragranular bubbles continues to increase with the burnup without prominent increase in bubble size. On the contrary, the number density of large bubbles only increases slightly, while the size of large bubbles keep increasing.

7.2 Hydrostatic Stress from BISON

Using the hydrostatic stress calculated by BISON may not yield precise gas swelling behavior as the hydrostatic stress is interrelated to the gas swelling behavior itself. But at least it shows the response of fuel to the restraints from cladding qualitatively. As shown in Figure 7.6, using hydrostatic stress from the BISON simulation, the gas swelling before the LOCA is approximately 0.6% lower than the zero stress case. After the LOCA, this difference increases to approximately 0.9%, showing the compressiblity of bubbles due to the restraints from the cladding. It is also worth mentioning that the difference between the two cases is not prominent until the burnup exceeds 20,000 MWD/MTW.

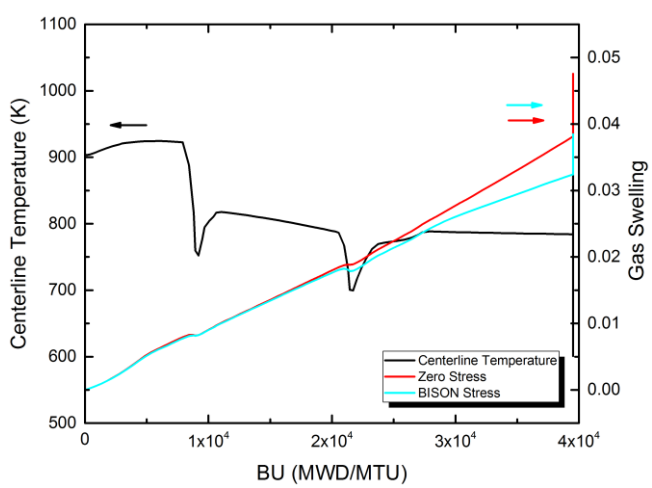

Figure 7.6 Comparison between zero stress and BISON stress conditions

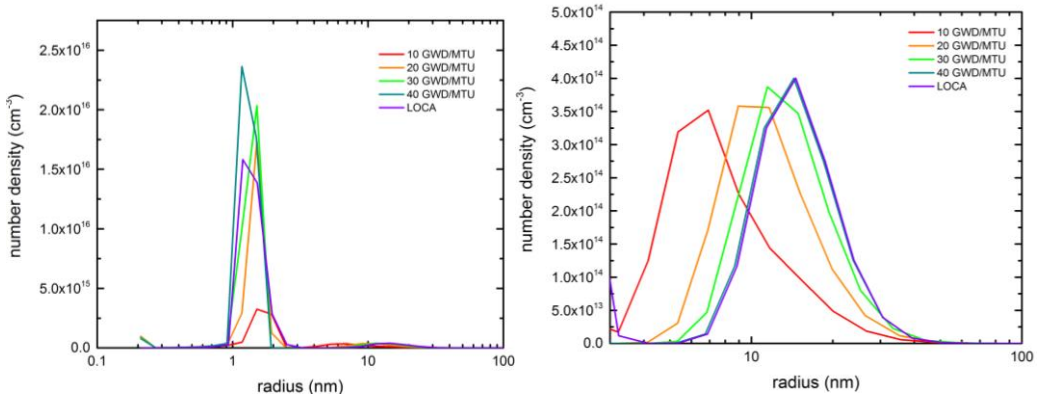

Figure 7.7 Intragranular bubble size distribution throughout the fuel life cycle with BISON-based stress (left) bubble size distribution from 0.2 nm to 100 nm in radius; (right) bubble size distribution near the large size peak.

A more detailed comparison was done by looking into the evolution of size distribution (see Figure 7.7). When the bubble size is small, the size distribution of the two cases are almost the same. As bubble size becomes larger than 10 nm in radius, the bubbles in the BISON stress case start to be compressible. This phenomenon is actually consistent with the fact that larger bubbles are easier to compress as implied by the hard sphere equation of state (EoS) used by GRASS-SST. As the LOCA occurs, the corresponding increase in the hydrostatic stress eliminates the majority of the bubble inflation due to the temperature increase.

Basically, this simulation with BISON stress shows that the cladding does help restrain the swelling as bubble size is large, especially after the LOCA. However, to get quantitative data, the swelling correlation used by BISON needs to be replaced by GRASS-SST rate theory model or at least some database derived from the GRASS-SST results.

8. Conclusions

In this study, we optimized the parameter for U_3Si_2 fuel based on coordinated efforts of state-of-the-art DFT calculations and low temperature irradiation experiments. The optimized parameters were utilized for the RT simulation based on the GRASS-SST code to predict the fuel performance of U_3Si_2 at LWR conditions. Multiple peripheral models were taken into consideration to cover majorly the cladding-fuel interaction effects. Both the swelling behavior and the fission gas bubble distribution were predicted by the RT model. At LWR conditions, the RT model predicts that intragranular bubbles dominate the swelling behavior. Aside from the steady-state modeling, the fission gas behavior in U_3Si_2 at a 70-second LOCA was also evaluated based on the development of the power transient related parameters as well as the BISON simulation based conditions. At LOCA, the majority of the swelling increase is contributed by the growth of overpressurized bubbles due to themal inflation, whereas coalescence of small bubbles also occurs. The fission gas bubbles remain intragranular and the extra swelling can be retained by cladding at LOCA. Further computational and experimental efforts are encouraged to improve the RT model. U_3Si_2 shows controllable fission gas behavior during steady-state operation and LOCA. In order to further evaluate the fuel performance and accident tolerance of U_3Si_2, the parameters should be further optimized, especially for the intergranular bubble models. On the other hand, longer LOCA simulation from the BISON simulation is also wanted for evaluation of accident tolerance in a longer term.

9. Acknowledgements

This work was funded by the U.S. Department of Energy (DoE)'s Nuclear Energy Advanced Modeling and Simulation (NEAMS) program. The efforts involving Argonne National Laboratory were supported under Contract No. DE-AC02-06CH11357 between UChicago Argonne, LLC and the U.S. Department of Energy.

10. References

[1] J. Rest, "GRASS-SST: a comprehensive mechanistic model for the prediction of fission-gas behavior in UO2-base fuels during steady-state and transient conditions," NUREG/CR-0202, Argonne National Laboratory, Report ANL-78-53 (1978)

[2] C. Ronchi, J. Nucl. Mater. 96 (1981) 314-328

[3] G.L. Hofman and Woo-Seog Ryu, "Detailed analysis of uranium silicide dispersion fuel swelling", Proceedings of the RERTR International Meeting, (1989)

[4] D.F. Sears, "Development and irradiation testing of Al-U_3Si_2 fuel at Chalk River Laboratories", Proceedings of the RERTR International Meeting, (1991)

[5] Y. Miao, B. Ye, Z.-G. Mei, G. Hofman, and A.M. Yacout, ANL Report NE-15/40, (2015)

[6] K.E. Metzger, T.W. Knight, and R.L. Williamson, INL Report CON-13-30445, (2014)

[7] H. Shimizu, Atomics International Report NAA-SR-10621, (1965)

[8] B. Watkins, D.S. Wood, "The significance of irradiation-induced creep on reactor performance of a Zircaloy-2 pressure tube," ASTM Selected Technical Papers, 458, 226-280 (1969)

[9] K.A. Gamble and J.D. Hales, "Preliminary Modeling of Accident Tolerant Fuel Concepts under Accident Conditions", Proceedings of Tope Fuel 2016 Conference, (2016)

Nuclear Engineering Division
Argonne National Laboratory
9700 South Cass Avenue, Bldg. 208
Argonne, IL 60439

www.anl.gov

Argonne National Laboratory is a U.S. Department of Energy
laboratory managed by UChicago Argonne, LLC